

Universal manuscript template for Optica Publishing Group journals

1. Abstract

2 Lorem ipsum ~100 words

3 2. Introduction

4 IR spectroscopy has seen significant interest and application in bio-imaging because it provides a
5 chemical fingerprint of underlying samples in a label-free way [1]. However, although the most
6 relevant chemical information can be gathered in the mid-infrared ($\sim 3 - 12 \mu\text{m}$), slow signal
7 acquisition is often a limiting factor, whose trade-off can keep it from competing with label-based
8 fluorescence microscopy.

9 Fig. 1 attempts to visualize the significant developments that have been made in mid-infrared
10 hyperspectral imaging over roughly the last two decades. Experiments are mapped onto the
11 two important metrics of spectra acquisition speed, which captures the rate at which spectra
12 are gathered, and optical bandwidth, which captures the breadth of chemical content that can
13 be observed. The two variables are plotted against each other, since a significant difficulty lies
14 in achieving both metrics simultaneously. For a better one to one comparison, the acquisition
15 speeds listed for experiments that use focal plane arrays have been normalized to that of an
16 analogous point scanning experiment.
17

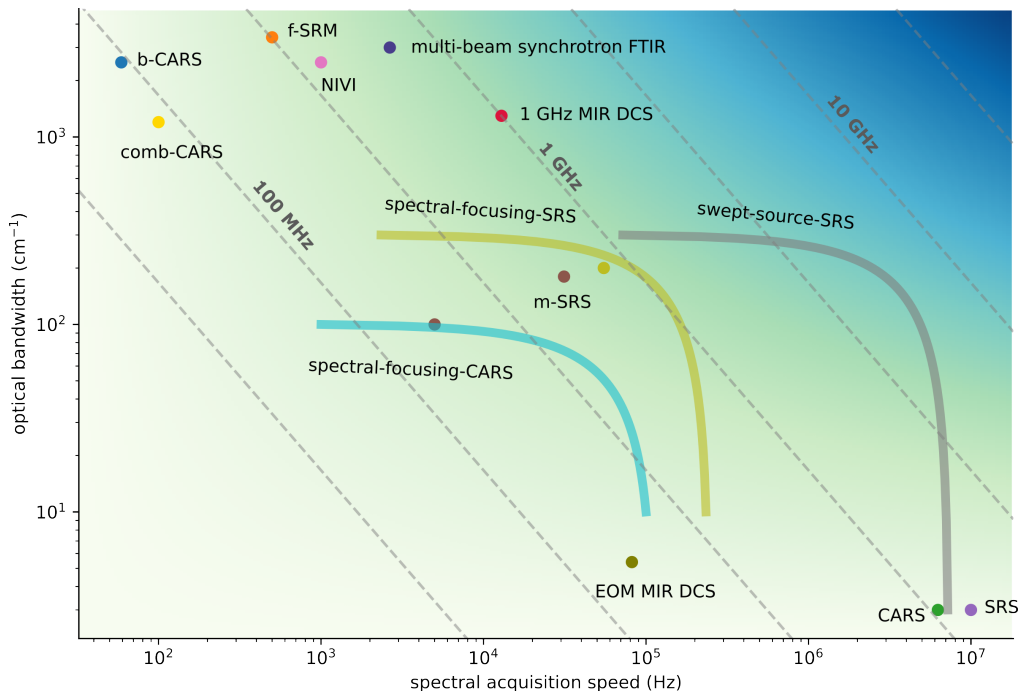


Fig. 1. Performance map of mid-infrared hyperspectral imaging. Broadband CARS (b-CARS) [2], femtosecond Stimulated Raman Microscopy (f-SRM) [3], in-vivo video rate CARS [4], in-vivo video rate SRS [5], multiplexed SRS (m-SRS) [6, 7], nonlinear interferometric vibrational imaging (NIVI) [8], swept-source SRS [9], spectral-focusing SRS [10], spectral-focusing CARS [11], spectral-focusing SRS [12], comb-CARS [13], multi-beam synchrotron FTIR [14], electro-optic modulator comb MIR DCS [15]

19 A few of the most notable experiments have utilized coherent Raman spectro-imaging, where
 20 in-vivo video-rate speeds have been demonstrated in the mid-infrared [4, 5]. Whereas initial
 21 demonstrations were over a narrow bandwidth ($\sim 3 \text{ cm}^{-1}$), broad bandwidths at high acquisition
 22 speeds have been demonstrated using rapidly rotating polygonal mirror scanners [12, 16]. However,
 23 the stated metrics are only possible with the strong Raman absorption cross-sections around
 24 2900 cm^{-1} , which precludes Raman spectroscopy-based platforms from achieving the same
 25 performance in the fingerprint region at longer wavelengths.

26 Conversely, Fourier transform spectroscopy (FTS) and quantum cascade laser (QCL) based
 27 imaging are attractive due to their broad applicability across the mid to long wavelength infrared.
 28 The high absorption cross-sections can also alleviate the need for operation at powers close to
 29 sample-damage thresholds, a concern that is applicable to biological samples. In this category,
 30 FTS spectrometers coupled to broadband and bright sources such as synchrotron facilities have
 31 set the state of the art for the combination of spectral bandwidth and speed [14]. The coupling of
 32 broadband synchrotron light into a microscope requires the active stabilization of a beam bundle.
 33 However, a widely accessible imaging method would benefit from having a simple and table
 34 top setup. QCL lasers are attractive due to their direct emission in the mid-infrared and small
 35 footprint, although their performance is best leveraged in narrowband applications. Tunable QCL
 36 packages consisting of multiple QCL chips combined into one device [17] can nominally reach
 37 broad spectral coverage, but struggle to reach noise figures comparable to platforms based on
 38 mode-locked lasers.

39 More recently, dual-comb spectroscopy (DCS) in the frequency comb community has become
 40 a popular platform, due to its improved stability and speed when compared to classical FTS [18].
 41 In this modality, the interference of two frequency combs maps a Nyquist band from the optical
 42 domain down into the RF. One of the most important considerations in DCS is the direct trade-off
 43 between the frequency resolution/repetition rate f_r and the size of the optical Nyquist window
 44 $\Delta\nu$:

$$\Delta\nu = \frac{f_r^2}{2\Delta f_r} \quad (1)$$

45 where Δf_r is the interferogram acquisition rate equal to the difference of the two laser repetition
 46 rates. The diagonal dashed lines in Fig. 1., show the $f_r^2/2$ trade-off between resolvable bandwidth
 47 and acquisition speed in DCS for different repetition rates. Evidently, when broad absorption
 48 features allow for coarse resolution, the highest repetition rates are desired. However, in order
 49 to reach sufficient power per comb tooth, in practice the pulse energy required for nonlinear
 50 frequency down-conversion from the near-infrared sets an upper limit on the obtainable repetition
 51 rate. In this work, we utilize a set of recently developed 1-GHz mid-infrared frequency combs [19]
 52 to integrate a dual-comb spectrometer with a confocal microscope. We capitalize on the high
 53 repetition rate by fully filling the third Nyquist band (2595 cm^{-1} – 3890 cm^{-1} at $\Delta f_r = 12.86 \text{ kHz}$).
 54 The system is among the fastest performers in the class of spectrometers covering over 1000 cm^{-1}
 55 with high spectral resolution in the mid-infrared.

56 However, pointing to the dashed line in the upper right corner of Fig. 1, in order to achieve the
 57 ultimate goal of label-free broadband video-rate imaging, we note that the ideal DCS platform
 58 would operate with repetition rates of 10 GHz or higher. Such systems would likely require either
 59 high-power amplifiers or a nanophotonic design capable of generating equivalent bandwidths in
 60 the mid-infrared with pump pulse energies around 100 pJ.

61 **3. Experiment**

62 With long-term stability in mind, a single-branch intra-pulse difference frequency generation
 63 (DFG) design is used to generate light in the mid-infrared [19]. Shown in Fig. 2, to compensate
 64 for the low conversion efficiency of the single-branch design, octave spanning few cycle NIR

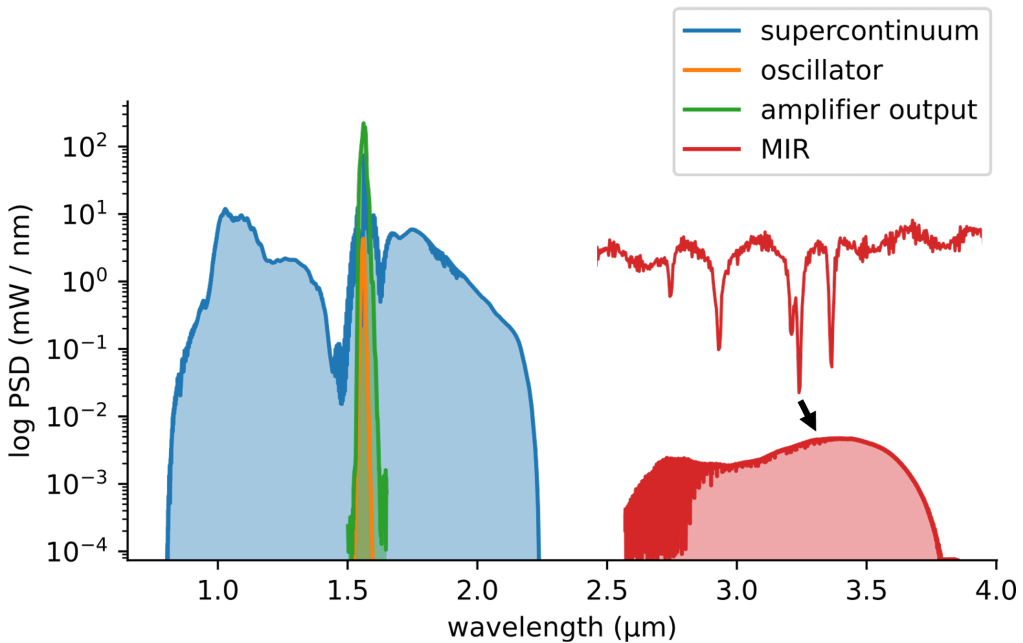


Fig. 2. 1 GHz MIR Frequency Comb. The spectral evolution through successive stages of the system: oscillator → chirped-pulse amplifier → few-cycle supercontinuum generation → MIR frequency down conversion. The inset shows a zoom in of waterlines that are resolved when using the full 1 GHz frequency resolution.

65 pulses generated via soliton self-compression in anomalous dispersion highly nonlinear fiber are
 66 used to drive the nonlinear frequency down conversion to the mid-infrared. Although coverage
 67 of the 6-12 μm wavelength region can be achieved for one laser system, due to the lack of
 68 nonlinear crystals in this work more widely available lithium niobate is used to cover the 3 - 5
 69 μm wavelength window.

70 Two 1-GHz mid-infrared frequency combs are generated and coupled into InF_3 single-mode
 71 fiber for delivery to the experiment. The output beam is collimated with a two inch off-axis
 72 parabolic mirror, and a reflective confocal microscope with 0.58 NA is used to image the beam
 73 onto a glass slide ($\sim 3.8 \mu\text{m}$ pixel size). A set of linear translation stages are used to raster scan
 74 the sample. The data is acquired via trigger, with the trigger spacing and scan speed set by the
 75 desired spatial sampling interval. The scan speed is limited only by the interferogram acquisition
 76 time, which is fundamentally set by the repetition rate of the laser. The transmitted signal is
 77 focused onto a high-speed MCT detector, whose AC coupled port is digitized at 1 GS/s using an
 78 FPGA. The data is streamed concurrently from the card memory into PC RAM for real-time
 79 analysis, and such that the card-memory does not limit the data volume. Owing to the fairly high
 80 500 MHz Nyquist frequency, and the placement of all fiber amplifiers in loop for the phase-locks
 81 of the two frequency combs, over one thousand interferograms can be directly averaged before
 82 phase correction needs to be employed.

83 4. Results

84 As a demonstration, hyperspectral images are taken of a USAF resolution target composed of
 85 SU-8 photoresist patterned onto a 500 μm thick Silicon wafer. Five hundred spectra (39 ms) are
 86 averaged at each pixel and apodized to 100 GHz (3.3 cm^{-1}). Point spectra shown in Fig. 4.(b).
 87 are taken at each pixel to generate the hypercube. The images are generated by integrating a

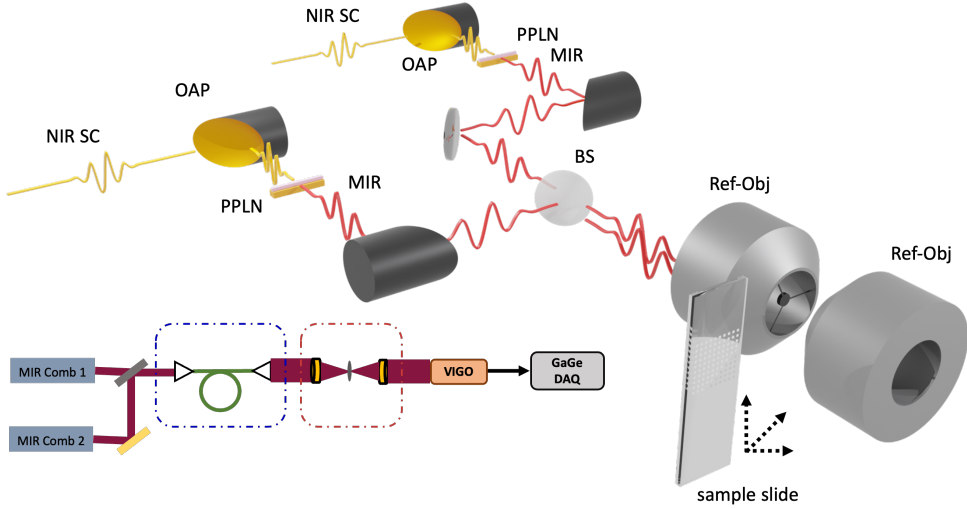


Fig. 3. Experimental Setup. Two mid-infrared frequency combs generated through intra-pulse difference frequency generation are passed collinearly through a confocal microscope. Hyperspectral images are collected by raster scanning the sample slide. The transmitted signal is collected and digitized in a high-speed MCT mid-infrared detector and FPGA.

88 ~63 cm⁻¹ window around the peak absorption at ~2930 cm⁻¹.

89 For a biologically relevant sample, we image a cross-section of ovarian cancer tissue (... add
90 info), where the paraffin wax was removed prior to dual-comb imaging. Five hundred spectra are
91 again averaged at each pixel and apodized to 3.3 cm⁻¹. Point spectra shown by the orange curve
92 in Fig. 5.(b). are taken at each pixel, with the two C-H anti-symmetric stretch bands visible at
93 2850 and 2920 cm⁻¹. A DCS spectrum taken with two second averaging time (25,700 averages)
94 is shown by the green curve, and a comparison spectrum taken using a commercial FTIR at
95 7.61 cm⁻¹ frequency resolution (... add info) is shown in the red curve. Apart from a broadening
96 of the peak, good qualitative agreement is observed between the DCS and FTIR hyperspectral
97 data. The FTIR image was taken prior to the removal of paraffin wax, which accounts for
98 the broadening of the peaks when compared to the spectra taken using DCS. The images are
99 generated by taking a slice through the hypercube at the peak of the 2920 cm⁻¹ band.

100 5. DCS Imaging Speed

101 Regardless of the imaging method, the final determination of imaging speed is given by the time
102 needed to reach sufficient SNR at each pixel. Specifically for DCS microscopy, the target SNR
103 and frequency resolution sets the pixel dwell time. In DCS, the absorbance noise σ scales with
104 the frequency resolution and number of averaged spectra N_{avg} according to [20]:

$$\sigma \propto \frac{N}{\sqrt{N_{avg}}} \quad (2)$$

105 where N is the number of frequency bins. This scaling rule is shown in Fig. 6.(c-d.), where it
106 is observed to match the experimentally measured absorbance noise. The two-variable map in
107 Fig. 6.(d). should apply more generally to any DCS point scanning microscopy, but with the
108 time axis scaled accordingly to the repetition rate.

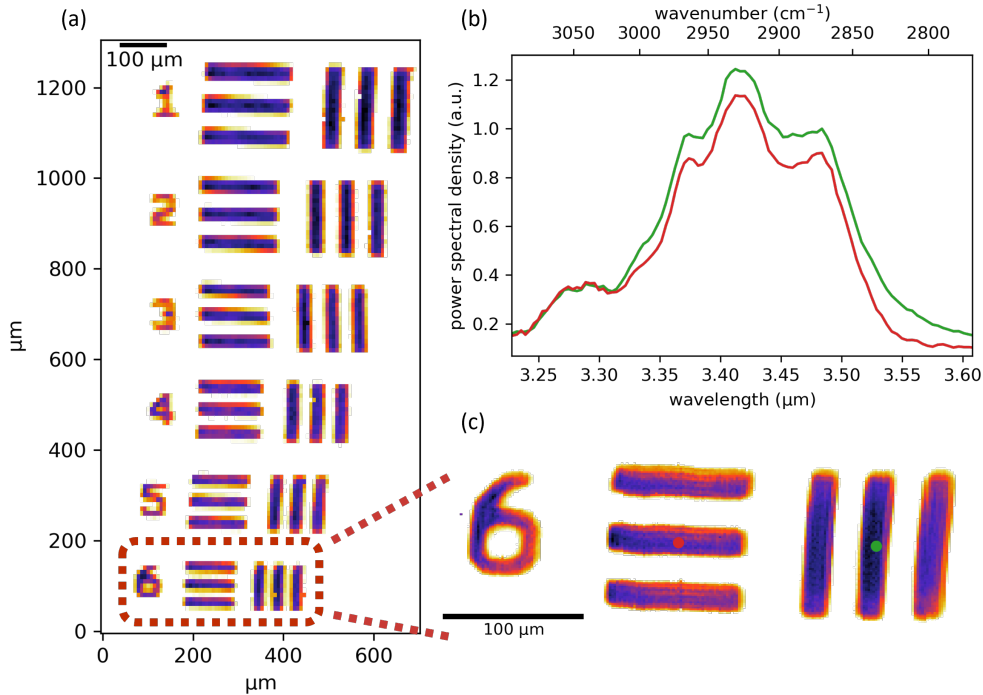


Fig. 4. Caption

109 Shown in Fig. 6.(a.), a baseline for 1 GHz DCS is that a 1000 cm^{-1} Nyquist window can be
 110 covered with ~ 17 kHz spectra acquisition speed, which is a two order magnitude improvement
 111 over well established 100 MHz mid-infrared dual-comb systems. In Fig. 6.(b.), a single-shot
 112 spectrum ($77\ \mu\text{s}$) at 1-GHz has low signal to noise, but can be averaged to high SNR in two
 113 seconds ($>25,000$ spectra). However, a high SNR can be achieved in ~ 39 ms at 500 averages if
 114 the interferograms are apodized to 100 GHz ($\sim 3.33\text{ cm}^{-1}$). The SNR as a function of averaging
 115 time and frequency resolution is shown in Fig. 6.(c-d);; the absorbance noise always averages
 116 down according to $1/\sqrt{N_{avg}}$, but with coarser resolution resulting in a directly proportional
 117 overall noise reduction.

118 References

- 119 1. M. J. Baker, J. Trevisan, P. Bassan, R. Bhargava, H. J. Butler, K. M. Dorling, P. R. Fielden, S. W. Fogarty, N. J.
 120 Fullwood, K. A. Heys, C. Hughes, P. Lasch, P. L. Martin-Hirsch, B. Obinaju, G. D. Sockalingum, J. Sulé-Suso, R. J.
 121 Strong, M. J. Walsh, B. R. Wood, P. Gardner, and F. L. Martin, "Using Fourier transform IR spectroscopy to analyze
 122 biological materials," *Nat. Protoc.* **9**, 1771–1791 (2014).
- 123 2. T. W. Kee and M. T. Cicerone, "Simple approach to one-laser, broadband coherent anti-Stokes Raman scattering
 124 microscopy," *Opt. Lett.* **29**, 2701 (2004).
- 125 3. E. Ploetz, S. Laimgruber, S. Berner, W. Zinth, and P. Gilch, "Femtosecond stimulated Raman microscopy," *Appl.
 126 Phys. B* **87**, 389–393 (2007).
- 127 4. C. L. Evans, E. O. Potma, M. Puoris'haag, D. Côté, C. P. Lin, and X. S. Xie, "Chemical imaging of tissue *in vivo* with
 128 video-rate coherent anti-Stokes Raman scattering microscopy," *Proc. National Acad. Sci.* **102**, 16807–16812 (2005).
- 129 5. B. G. Saar, C. W. Freudiger, J. Reichman, C. M. Stanley, G. R. Holtom, and X. S. Xie, "Video-Rate Molecular
 130 Imaging in Vivo with Stimulated Raman Scattering," *Science* **330**, 1368–1370 (2010).
- 131 6. D. Fu, F.-K. Lu, X. Zhang, C. Freudiger, D. R. Pernik, G. Holtom, and X. S. Xie, "Quantitative Chemical Imaging
 132 with Multiplex Stimulated Raman Scattering Microscopy," *J. Am. Chem. Soc.* **134**, 3623–3626 (2012).
- 133 7. C.-S. Liao, M. N. Slipchenko, P. Wang, J. Li, S.-Y. Lee, R. A. Oglesbee, and J.-X. Cheng, "Microsecond scale
 134 vibrational spectroscopic imaging by multiplex stimulated Raman scattering microscopy," *Light. Sci. & Appl.* **4**,

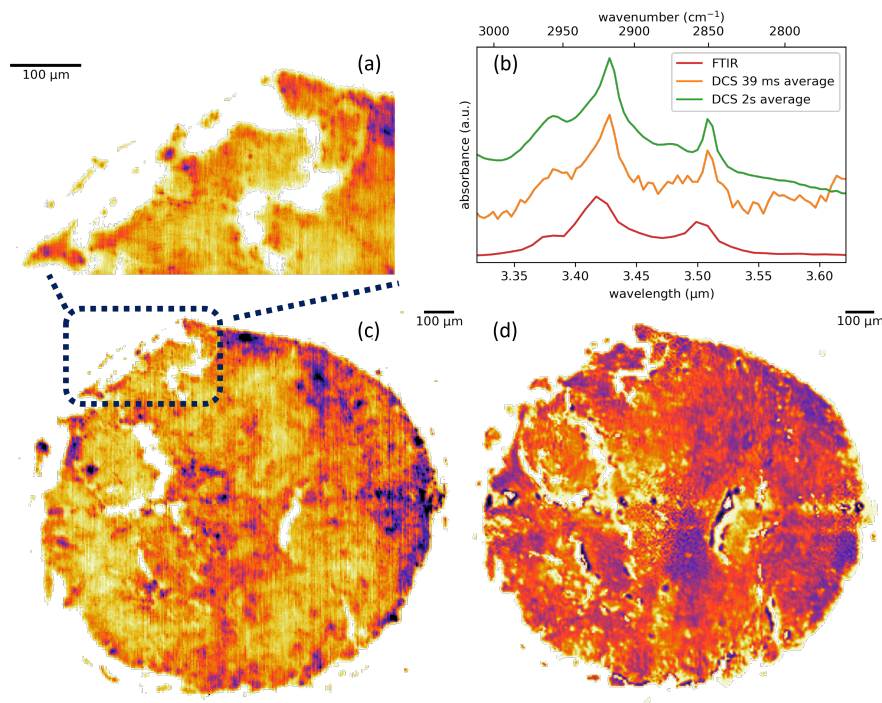


Fig. 5. Caption

- 135 e265–e265 (2015).
- 136 8. P. D. Chowdary, Z. Jiang, E. J. Chaney, W. A. Benalcazar, D. L. Marks, M. Gruebele, and S. A. Boppart, “Molecular
137 Histopathology by Spectrally Reconstructed Nonlinear Interferometric Vibrational Imaging,” *Cancer Res.* **70**,
138 9562–9569 (2010).
- 139 9. Y. Ozeki, W. Umemura, Y. Otsuka, S. Satoh, H. Hashimoto, K. Sumimura, N. Nishizawa, K. Fukui, and K. Itoh,
140 “High-speed molecular spectral imaging of tissue with stimulated Raman scattering,” *Nat. Photonics* **6**, 845–851
141 (2012).
- 142 10. D. Fu, G. Holtom, C. Freudiger, X. Zhang, and X. S. Xie, “Hyperspectral Imaging with Stimulated Raman Scattering
143 by Chirped Femtosecond Lasers,” *The J. Phys. Chem. B* **117**, 4634–4640 (2013).
- 144 11. C. Di Napoli, I. Pope, F. Masia, P. Watson, W. Langbein, and P. Borri, “Hyperspectral and differential CARS
145 microscopy for quantitative chemical imaging in human adipocytes,” *Biomed. Opt. Express* **5**, 1378 (2014).
- 146 12. H. Lin, H. J. Lee, N. Tague, J.-B. Lugagne, C. Zong, F. Deng, J. Shin, L. Tian, W. Wong, M. J. Dunlop, and J.-X.
147 Cheng, “Microsecond fingerprint stimulated Raman spectroscopic imaging by ultrafast tuning and spatial-spectral
148 learning,” *Nat. Commun.* **12**, 3052 (2021).
- 149 13. T. Ideguchi, S. Holzner, B. Bernhardt, G. Guelachvili, N. Picqué, and T. W. Hänsch, “Coherent Raman spectro-imaging
150 with laser frequency combs,” *Nature* **502**, 355–358 (2013).
- 151 14. M. J. Nasse, M. J. Walsh, E. C. Mattson, R. Reininger, A. Kajdacsy-Balla, V. Macias, R. Bhargava, and C. J.
152 Hirschmugl, “High-resolution Fourier-transform infrared chemical imaging with multiple synchrotron beams,” *Nat.
153 Methods* **8**, 413–416 (2011).
- 154 15. F. Ullah Khan, G. Guarnizo, and P. Martín-Mateos, “Direct hyperspectral dual-comb gas imaging in the mid-infrared,”
155 *Opt. Lett.* **45**, 5335 (2020).
- 156 16. M. Tamamitsu, Y. Sakaki, T. Nakamura, G. K. Podagatlapalli, T. Ideguchi, and K. Goda, “Ultrafast broadband
157 Fourier-transform CARS spectroscopy at 50,000 spectra/s enabled by a scanning Fourier-domain delay line,” *Vib.
158 Spectrosc.* **91**, 163–169 (2017).
- 159 17. K. Yeh, S. Kenkel, J.-N. Liu, and R. Bhargava, “Fast Infrared Chemical Imaging with a Quantum Cascade Laser,”
160 *Anal. Chem.* **87**, 485–493 (2015).
- 161 18. I. Coddington, N. Newbury, and W. Swann, “Dual-comb spectroscopy,” *Optica* **3**, 414 (2016).
- 162 19. N. Hoghooghi, S. Xing, P. Chang, D. Lesko, A. Lind, G. Rieker, and S. Diddams, “Broadband 1-GHz mid-infrared
163 frequency comb,” *Light. Sci. & Appl.* **11**, 264 (2022).
- 164 20. N. R. Newbury, I. Coddington, and W. Swann, “Sensitivity of coherent dual-comb spectroscopy,” *Opt. Express* **18**,

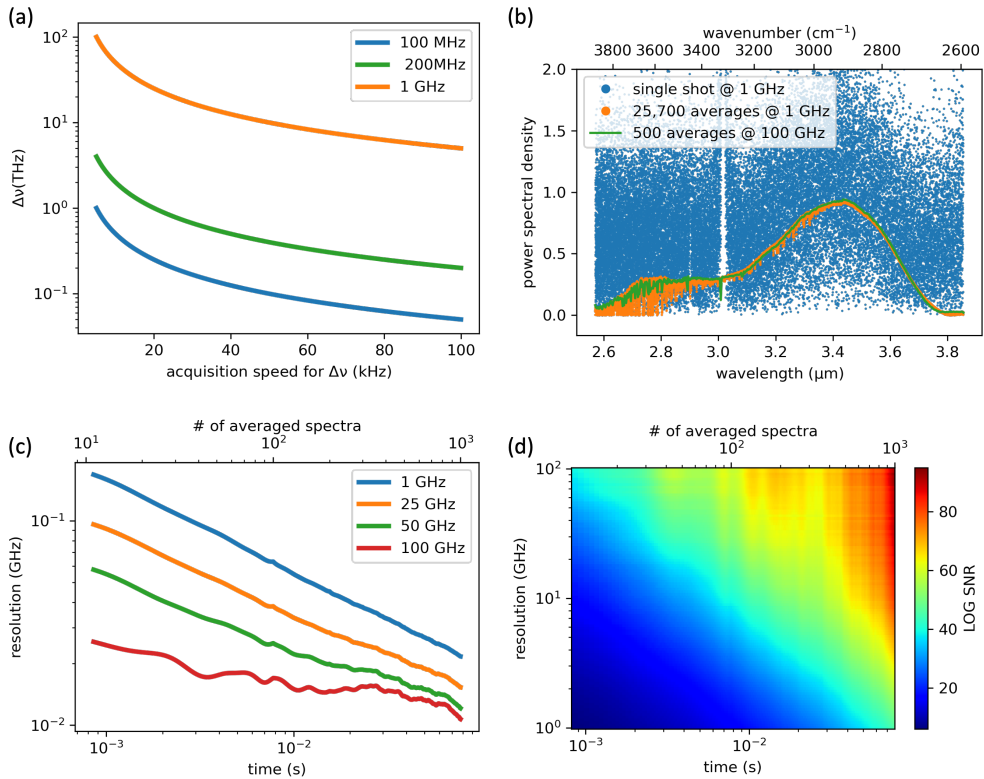


Fig. 6. Summary of DCS Imaging Speed. (a) The size of the optical Nyquist window plotted against acquisition speed (Δf_r) for different repetition rates. (b) DCS spectrum taken at different averaging times and frequency resolution/apodization windows. (c) The spectra's SNR follow the scaling of Eq.2, with an example of the 2D parameter space (d) mapped out for the 1-GHz system.